Progress In Electromagnetics Research, Vol. 120, 439–457, 2011

CONVERGENCE STUDY OF A NON-STANDARD SCHWARZ DOMAIN DECOMPOSITION METHOD FOR FINITE ELEMENT MESH TRUNCATION IN ELECTROMAGNETICS

R. Fernandez-Recio[1], L. E. Garcia-Castillo[2,*], S. Llorente-Romano[2], and I. Gomez-Revuelto[3]

[1]Detectability and Electronic Warfare Laboratory, INTA, National Institute of Aerospace Technology, Spain

[2]Departamento de Teoría de la Señal y Comunicaciones, Universidad Carlos III de Madrid, Leganés, Madrid, Spain

[3]Departamento de Ingeniería Audiovisual y Comunicaciones, Universidad Politécnica de Madrid, Madrid 28031, Spain

Abstract—A convergence study of a non-standard Schwarz domain decomposition method for finite element mesh truncation in electromagnetics is carried out. The original infinite domain is divided into two overlapping domains. The interior finite domain is modeled by finite elements and the exterior infinite domain by an integral equation representation of the field. A numerical study of the spectrum of the iteration matrix for non-convex mesh truncation boundaries is performed. The projection of the error between two consecutive iterations onto the eigenvector space of the iteration matrix is performed. The numerical results explain the observed convergence behavior of the Schwarz iterations.

1. INTRODUCTION

In this paper, a convergence study of a non-standard Schwarz domain decomposition method for finite element mesh truncation in electromagnetics is presented. The method is named Finite Element-Iterative Integral Equation Evaluation (FE-IIEE). The original infinite domain is divided into two overlapping domains. The term "non-standard" refers to the fact that each domain is analyzed using a

Received 21 July 2011, Accepted 19 September 2011, Scheduled 29 September 2011

* Corresponding author: Luis E. Garcia-Castillo (luise@tsc.uc3m.es).

different technique. The interior finite domain is modeled by the Finite Element Method (FEM) [1–4] using a Cauchy (Robin) type of boundary condition for the mesh truncation boundary. The exterior infinite domain is modeled by an integral equation representation of the field [5–8]. According to Schwarz theory, the solution is obtained through an iterative process in which the radiation boundary condition on the mesh truncation boundary is updated.

The Schwarz methodology object of the paper has been applied successfully by different authors (including the ones of this paper) to radiation and scattering problems in two dimensions (2D) and three dimensions (3D) of different forms; eg., hybridized or not with high frequency techniques (see [9–11], and the references therein) using non-conformal coupling [12], together with p-adaptivity [13], and within multi-region iterative strategies [14–16].

A previous theoretical study of the convergence of the mentioned Schwarz methodology for scattering problems in 2D is found in [17]. A theoretical condition to assure the convergence of the method for the case of a circular mesh truncation boundary is obtained: the truncation boundary must be placed at a distance greater than a minimum one from the scatter (typically very close from the surface of the scatter). Moreover, as the overlapping between the two domains is larger, faster rates of convergence are found. However, the number of unknowns increase with the FEM domain. This suggests a compromise in the placement of the truncation boundary if computing time is a concern. Similar conclusions were obtained for the 3D case in [12]. The authors have observed the same type of behavior for a wide variety of problems in 2D and 3D making use of different convex truncation boundaries. However, problems with non-convex boundaries (useful for scatters with reentrant corners in order to minimize the number of unknowns) does not follow the convergence behavior described above. In this paper, the issue of the convergence of the method for non-convex truncation boundaries is addressed. Specifically, this issue is illustrated through the example of the scattering of a plane wave inciding on a metallic open cavity in which the truncation boundary is chosen conformal to the cavity. It is worth noting that some preliminary results were presented in a conference paper, [18]. In the present full paper, further numerical results are presented and more importantly detailed comments about the results and the pertinent conclusions are given.

The rest of the paper is organized as follows: Section 2 describes briefly the iterative FEM methodology and how the convergence analysis is performed. Numerical results are provided in Section 3. Thereafter, we remark on the main conclusions.

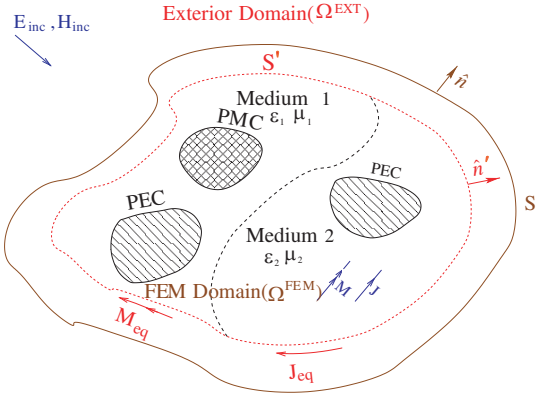

Figure 1. Domain decomposition of the open region problem.

2. ITERATIVE FEM METHODOLOGY FE-IIEE

Figure 1 depicts a typical problem setup. The original infinite domain is divided into two overlapping domains: a FEM domain (Ω^{FEM}) bounded by the surface S and the infinite domain exterior to the auxiliary boundary S' (Ω^{EXT}). Thus, the overlapping region is limited by S' and S. For simplicity, the region exterior to S is assumed to be a homogeneous medium. The boundary S may be arbitrarily shaped but typically it is selected to be conformal to S'. Distance from S' to S is usually small, typically in the range of 0.05λ to 0.2λ. Thus, the FEM domain can be truncated very close to the sources of the problem reducing the number of unknowns of the problem.

2.1. Formulation

An algebraic system of equations characterizing electromagnetically Ω^{FEM} is obtained by using FEM. Specifically, the implementation is based on the double curl vector wave equation in terms of the electric (**E**) or magnetic (**H**) field [2]:

$$\boldsymbol{\nabla} \times \left(\bar{\bar{f}}_r^{\,-1} \boldsymbol{\nabla} \times \mathbf{V} \right) - k_0^2 \, \bar{\bar{g}}_r \mathbf{V} = \mathbf{q} \quad \text{in } \Omega \tag{1}$$

where k_0 is the wavenumber in vacuum and $\mathbf{q} = -jk_0 h_0 \mathbf{O} - \boldsymbol{\nabla} \times (\bar{\bar{f}}_r^{-1} \mathbf{L})$ is the source term due to the presence of impressed electric and/or magnetic currents within Ω. See Table 1 for the different magnitudes involved in the **E** and **H** formulations.

Boundary conditions of Perfect Electric Conductor (PEC) and Perfect Magnetic Conductor (PMC), i.e., homogeneous Dirichlet or

Table 1. Formulation magnitudes and parameters.

	$\mathbf{V}$	$\bar{\bar{f}}_r$	$\bar{\bar{g}}_r$	h	$\mathbf{O}$	$\mathbf{L}$	Γ_D	Γ_N
Form. $\mathbf{E}$	$\mathbf{E}$	$\bar{\bar{\mu}}_r$	$\bar{\bar{\varepsilon}}_r$	η	$\mathbf{J}$	$\mathbf{M}$	Γ_{PEC}	Γ_{PMC}
Form. $\mathbf{H}$	$\mathbf{H}$	$\bar{\bar{\varepsilon}}_r$	$\bar{\bar{\mu}}_r$	$\frac{1}{\eta}$	$\mathbf{M}$	$-\mathbf{J}$	Γ_{PMC}	Γ_{PEC}

Neumann type boundary conditions on Γ_D and Γ_N may be used according to Table 1. The formulation also handles the presence of waveguide ports by means of a multi-mode boundary condition, but the details are omitted as they are not relevant to the objectives of the paper.

A local type boundary condition is used on S, specifically the Cauchy boundary condition:

$$\hat{\mathbf{n}} \times \left(\frac{1}{f_r} \boldsymbol{\nabla} \times \mathbf{V} \right) + j \frac{k}{f_r} \hat{\mathbf{n}} \times \hat{\mathbf{n}} \times \mathbf{V} = \boldsymbol{\Psi} \quad \text{at } \Gamma_S \tag{2}$$

where $\hat{\mathbf{n}}$ is the outward unit vector normal to S and k is the wavenumber of the medium exterior to S', assumed to be homogeneous.

Thus, the variational formulation of the problem is:

Find $\mathbf{V} \in \mathbf{W}$ such that

$$c(\mathbf{F}, \mathbf{V}) = l(\mathbf{F}), \qquad \forall \mathbf{F} \in \mathbf{W} \tag{3}$$

where the bilinear and linear forms, $c(\mathbf{F}, \mathbf{V})$ and $l(\mathbf{F})$, are defined as follows

$$\begin{aligned} c(\mathbf{F}, \mathbf{V}) &= \int_\Omega (\boldsymbol{\nabla} \times \mathbf{F}) \cdot \left(\bar{\bar{f}}_r^{\,-1} \boldsymbol{\nabla} \times \mathbf{V} \right) d\Omega - k_0^2 \int_\Omega \mathbf{F} \cdot \bar{\bar{g}}_r \mathbf{V} d\Omega \\ &\quad + j \frac{k}{f_r} \int_{\Gamma_S} (\hat{\mathbf{n}} \times \mathbf{F}) \cdot (\hat{\mathbf{n}} \times \mathbf{V}) d\Gamma \\ l(\mathbf{F}) &= \int_\Omega \mathbf{F} \cdot \mathbf{q} d\Omega + \int_{\Gamma_S} \mathbf{F} \cdot \boldsymbol{\Psi} d\Gamma \end{aligned} \tag{4}$$

with

$$\mathbf{W} := \{ \mathbf{A} \in \mathbf{H}(\text{curl}, \Omega),\ \hat{\mathbf{n}} \times \mathbf{A} = 0 \text{ on } \Gamma_D \} \tag{5}$$

and $\mathbf{H}(\text{curl})$ being the space of square integrable vector functions with square integrable curl.

The discretization of the above variational formulation using the second-order tetrahedra described in [2, 19] leads to a sparse system of equations that may be expressed in partitioned form as follows

$$\begin{bmatrix} K_{II} & K_{IS} \\ K_{SI} & K_{SS} \end{bmatrix} \begin{Bmatrix} \left\{ \phi_I^{(i)} \right\} \\ \left\{ \phi_S^{(i)} \right\} \end{Bmatrix} = \begin{Bmatrix} \{ b_I \} \\ \left\{ b_\Psi^{(i)} \right\} \end{Bmatrix} \tag{6}$$

where the superindex i denotes the value of the variables at the i-th iteration of the iterative process.

The sub-indexes S and I refer to the degrees of freedom g associated to S (i.e., associated to nodes on Γ_S) and those associated to nodes in the interior of S, respectively. Thus, the right hand side term $\{b_I\}$ corresponds to the discretization of the first term of $l(\mathbf{F})$ in (4). The term $\{b_\Psi\}$ corresponds to the discretization of the second term of $l(\mathbf{F})$ in (4).

The iterative process is started by fixing the initial value of function $\mathbf{\Psi}$, which is denoted in matrix form as $\{\Psi^{(0)}\}$. Typically, $\{\Psi^{(0)}\}$ is fixed to zero for radiation problems and to $\{\Psi^{\text{inc}}\}$ for scattering problems; $\{\Psi^{\text{inc}}\}$ being the result of introducing the incident field into expression (2). Then, the FEM system (6) is solved. A new value of $\{\Psi\}$, in general $\{\Psi^{(i+1)}\}$, is obtained by using the integral equation representation of the field in the infinite exterior domain. Thus, FEM fields on S' are calculated in order to compute the electric and magnetic current densities $\mathbf{J}_{\text{eq}}$ and $\mathbf{M}_{\text{eq}}$ of the equivalent exterior problem. The field $\mathbf{V}^{\text{IE-FEM}}$, and its curl $\boldsymbol{\nabla}\times\mathbf{V}^{\text{IE-FEM}}$, over S radiated by $\mathbf{J}_{\text{eq}}$ and $\mathbf{M}_{\text{eq}}$ are computed using the integral expressions:

$$\mathbf{V}^{\text{IE-FEM}} = \oiint_{S'} (\mathbf{L}_{\text{eq}} \times \boldsymbol{\nabla} G) dS' - jkh \oiint_{S'} \left(\mathbf{O}_{\text{eq}} \left(G + \frac{1}{k^2} \boldsymbol{\nabla}\boldsymbol{\nabla} G \right) \right) dS' \quad (7)$$

$$\boldsymbol{\nabla}\times\mathbf{V}^{\text{IE-FEM}} = jkh \oiint_{S'} (\mathbf{O}_{\text{eq}} \times \boldsymbol{\nabla} G) dS' - \oiint_{S'} \left(\mathbf{L}_{\text{eq}} \left(k^2 G + \boldsymbol{\nabla}\boldsymbol{\nabla} G \right) \right) dS' \quad (8)$$

where h stands for the immittance of the homogenous medium (see Table 1), and G denotes the Green's function for a homogeneous medium, $G \equiv G(\mathbf{r}, \mathbf{r}') = (1/(4\pi) \exp[-jk(\mathbf{r} - \mathbf{r}')]/(4\pi|\mathbf{r} - \mathbf{r}'|)$, which typically is the free space.

Finally, function $\{\Psi^{(i+1)}\}$ is computed by introducing the values of the fields $\mathbf{V}(\mathbf{r} \in \Gamma_S)$ and $\boldsymbol{\nabla} \times \mathbf{V}(\mathbf{r} \in \Gamma_S)$ in (2).

The just described procedure to update $\{b_\Psi\}$ may be compactly expressed in matrix form as follows:

$$\left\{ b_\Psi^{(i+1)} \right\} = [C] \left\{ \Psi^{(i+1)} \right\} = [C] \left\{ \Psi^{(0)} \right\} + [C] \left[M_I \, M_S \right] \left\{ \begin{array}{c} \left\{ \phi_I^{(i)} \right\} \\ \left\{ \phi_S^{(i)} \right\} \end{array} \right\} \quad (9)$$

where $[C]$ is a rectangular matrix that weighs the residual vector with the interpolating functions on S (linear form of (4)) and $[M]$ represents the integral operator given by the Green function (expressions (7) and (8)) together with action of combining the field and its curl into (2).

More details of the formulation and its implementation are given in [9, 10]. Work referenced in [9] is in the context of 2D problems

while [10] is for 3D problems. It is worth noting that the convergence study of the paper is performed in the context of 3D problems. However, the conclusions are valid for 2D and 3D applications.

2.2. Convergence Analysis

As a summary, the iterative FEM algorithm follows the algorithm given by expressions and (6), (9). The process stops when a certain error criterion based on the difference between $\{\Psi^{(i+1)}\}$ and $\{\Psi^{(i)}\}$ is satisfied. Substituting in (9) the degrees of freedom from (6):

$$\left\{b_\Psi^{(i+1)}\right\} = [C]\{\Psi^{(0)}\} + [B]\left\{\begin{array}{c}\{b_I\}\\ \left\{b_\Psi^{(i)}\right\}\end{array}\right\} = \{w\} + [B_\Psi]\left\{b_\Psi^{(i)}\right\} \quad (10)$$

where $\{w\} = [C]\{\Psi^{(0)}\} + [B_I]\{b_I\}$ is a vector that remains constant along all the iterations. Matrix $[B]$ has been defined as

$$[B] = [C]\,[\,M_I \;\; M_S]\begin{bmatrix}K_{II} & K_{IS}\\ K_{SI} & K_{SS}\end{bmatrix}^{-1} = [\,B_I \quad B_\Psi] \quad (11)$$

Spectrum of $[B_\Psi]$ determines the convergence of the iterative method and corresponds to the iteration matrix. According with the theory, the method converges if, and only if, the spectral radius of the iteration matrix, defined as the maximum absolute value of the matrix eigenvalues, is smaller than one. $\{b_\Psi^{(0)}\}$ corresponds to the initial iteration and can be written as the sum of two components: the true solution, $\{b_{\Psi_t}\}$, and the error one, $\{b_{\Psi_e}^{(0)}\}$, that is, $\{b_\Psi^{(0)}\} = \{b_{\Psi_t}\} + \{b_{\Psi_e}^{(0)}\}$. On the other hand, the degrees of freedom in the initial iteration can be written as:

$$\left\{\phi^{(0)}\right\} = [K]^{-1}\left\{\begin{array}{c}\{b_I\}\\ \{b_{\Psi_t}\}\end{array}\right\} + [K]^{-1}\left\{\begin{array}{c}0\\ \left\{b_{\Psi_e}^{(0)}\right\}\end{array}\right\} = \{\phi_t\} + \left\{\phi_e^{(0)}\right\} \quad (12)$$

where $\{\phi_t\}$ gives the true degrees of freedom and $\{\phi_e^{(0)}\}$ gives the error in the initial iteration of the estimation of the degrees of freedom. Once the degrees of freedom are obtained, $\{b_\Psi^{(1)}\}$, corresponding to the first iteration, can be written as

$$\left\{b_\Psi^{(1)}\right\} = \underbrace{[C]\left\{\Psi^{(0)}\right\} + [C][M]\{\phi_t\}}_{\{b_{\Psi_t}\}} + \underbrace{[C][M]\left\{\phi_e^{(0)}\right\}}_{\left\{b_{\Psi_e}^{(1)}\right\}} \quad (13)$$

where $\{b_{\Psi_e}^{(1)}\}$ is the error of $\{b_\Psi\}$ for the first iteration, which can be written as

$$\left\{b_{\Psi_e}^{(1)}\right\} = [C][M]\left\{\phi_e^{(0)}\right\} = [C][M][K]^{-1}\left\{\begin{array}{c} 0 \\ \left\{b_{\Psi_e}^{(0)}\right\} \end{array}\right\} = [B_\Psi]\left\{b_{\Psi_e}^{(0)}\right\} \quad (14)$$

The following expression can be found after m iterations

$$\left\{b_{\Psi_e}^{(m)}\right\} = [B_\Psi]^m\left\{b_{\Psi_e}^{(0)}\right\} \quad (15)$$

Therefore, the proposed methodology converges to the true solution, for any initial value $\{\Psi^{(0)}\}$, if and only if, the spectral radius of the iteration matrix $[B_\Psi]$ is less than one. Otherwise, the method may diverge.

Using (10), the residual error at the iterations $i+1$ and i can be written in terms of the previous iteration, respectively:

$$\left\{b_\Psi^{(i+1)}\right\} = \{w\} + [B_\Psi]\left\{b_\Psi^{(i)}\right\} \quad (16a)$$

$$\left\{b_\Psi^{(i)}\right\} = \{w\} + [B_\Psi]\left\{b_\Psi^{(i-1)}\right\} \quad (16b)$$

The following relation is found subtracting the Equations (16a) and (16b):

$$\left\{b_\Psi^{(i+1)}\right\} - \left\{b_\Psi^{(i)}\right\} = [B_\Psi]\left(\left\{b_\Psi^{(i)}\right\} - \left\{b_\Psi^{(i-1)}\right\}\right) \quad (17)$$

$$\left\{z^{(i+1)}\right\} = [B_\Psi]\left\{z^{(i)}\right\} \quad (18)$$

where $\{z^{(i)}\} = \{b_\Psi^{(i)}\} - \{b_\Psi^{(i-1)}\} = \{b_{\Psi_e}^{(i)}\} - \{b_{\Psi_e}^{(i-1)}\}$ represents the change of the residual error between two consecutive iterations and, therefore, the change of the error in $\{b_\Psi\}$. The change of the residual error in the first iteration can be projected onto the eigenvalues space of the iteration matrix $[B_\Psi]$ as $\{z^{(1)}\} = \sum_{j=1}^{n} c_j\{v_j\}$ where n is the dimension of the iteration matrix, $\{v_j\}$ is the j-th eigenvector and c_j its associated coefficient. In matrix notation, $\{z^{(1)}\}$ can be expressed as:

$$\left\{z^{(1)}\right\} = [V]\{c\} \quad (19)$$

where the columns of $[V]$ are the eigenvectors and $\{c\}$ is a vector that contains the mentioned coefficients. The change of the residual error in the second iteration can be written as:

$$\left\{z^{(2)}\right\} = [B_\Psi]\left\{z^{(1)}\right\} = [B_\Psi][V]\{c\} = [V]\{c'\} \quad (20)$$

where the component j of $\{c'\}$ is $c'_j = c_j\lambda_j$, and λ_j is the jth eigenvalue of the iteration matrix $[B_\Psi]$. Recursively, the projection of the ith change of the residual error between two consecutive iterations can be written as $\{z^{(i)}\} = \sum_{j=1}^{n} c_j\lambda_j^{(i-1)}\{v_j\}$.

3. NUMERICAL RESULTS

Let us consider a metallic scatterer consisting of a cavity type structure open on one of their sides. The dimensions of the interior cavity are $0.8\lambda \times 0.8\lambda \times 1\lambda$ with 0.1λ thick walls. The analysis of the scattering of a plane wave incident on that metallic open cavity is performed using the FE-IIEE methodology. Two types of mesh truncation strategies are

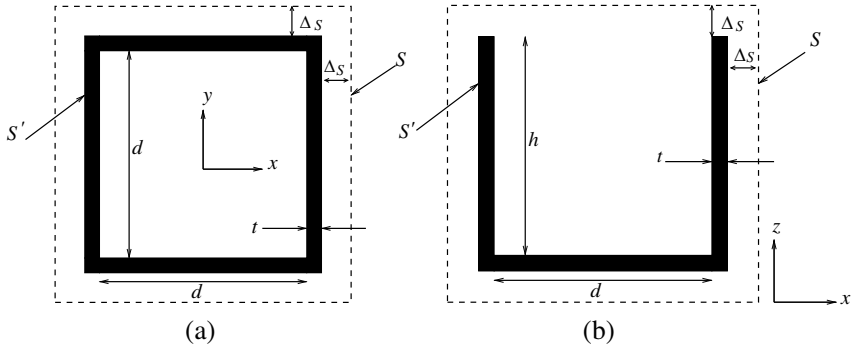

Figure 2. Mesh truncation for cavity problem (convex case). (a) Top view. (b) Side view.

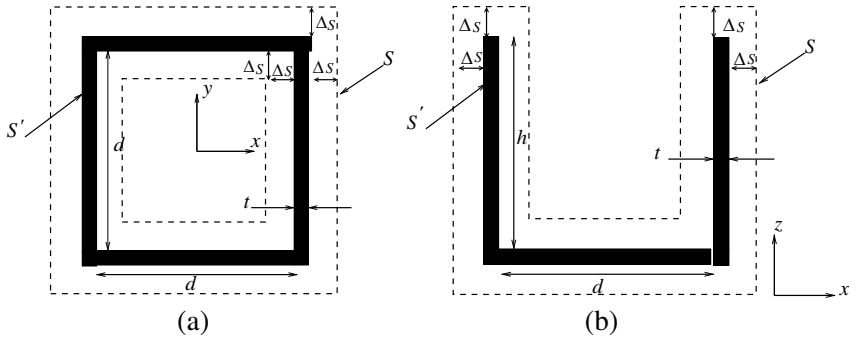

Figure 3. Mesh truncation for cavity problem (non-convex case). (a) Top view. (b) Side view.

considered. The first one uses a box-type mesh truncation boundary S for the problem (see Figure 2). Thus, a convex type of mesh truncation is applied. The second type of mesh truncation is the one shown in Figure 3, i.e., the exterior boundary S is chosen conformal to the cavity walls. Thus, a non-convex type of mesh truncation is applied. Actually, a strong re-entrant region is present for the truncation boundary in this case. The former type of mesh truncation is the one that should be chosen for the structure under considerarion in order to avoid convergence problems. The latter type of mesh truncation is deliberately used here in order to conclude about the convergence of FE-IIEE with non-convex boundaries and large re-entrant regions. Notice that in both cases the auxiliary boundary S' is chosen conformal to the object, i.e., S' is conformal to S with the exception of the top cover for the convex case (see Figure 2(b)). However, the convex or non-convex nature of surface S' has no impact in the convergence of the method.

In order to illustrate first the behavior of FE-IIEE with the usual convex type truncation boundary, two set of results have been chosen. The first results are shown in the plot of Figure 4. The plot represents the convergence behavior (change of the residual error — normalized — between two consecutive iterations) for different cases of mesh truncation setup implying different S-S' distances, i.e., different sizes for the overlapping region between Ω^{FEM} and Ω^{EXT} (see Table 2(a)). As expected, the larger the size of the overlapping region the better

Table 2. Cases of mesh truncation setup used in the paper. (a) Convex type. (b) Non-convex type.

	Truncation Boundary	Min. distance S-S'
$\mathcal{T}_1$	$1.1\lambda \times 1.1\lambda \times 1.2\lambda$	0.05λ
$\mathcal{T}_2$	$1.2\lambda \times 1.2\lambda \times 1.3\lambda$	0.1λ
$\mathcal{T}_3$	$1.3\lambda \times 1.3\lambda \times 1.4\lambda$	0.15λ
$\mathcal{T}_4$	$1.4\lambda \times 1.4\lambda \times 1.5\lambda$	0.2λ
$\mathcal{T}_5$	$1.5\lambda \times 1.5\lambda \times 1.6\lambda$	0.25λ
$\mathcal{T}_6$	$1.6\lambda \times 1.6\lambda \times 1.7\lambda$	0.3λ

(a)

	Distance S-S'
$\mathcal{A}$	0.1λ
$\mathcal{B}$	0.15λ

(b)

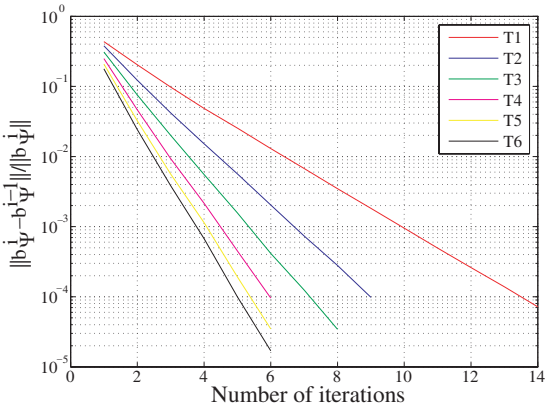

Figure 4. Convergence for different cases of mesh truncation (convex type) setup implying different S-S' distances. See Table 2(a). Case of $(\theta^{\text{inc}}, \phi^{\text{inc}}) = (0°, 0°)$.

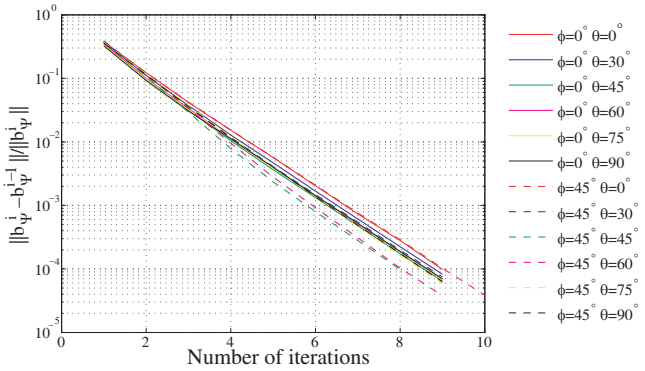

Figure 5. Convergence for different angles of incidence with convex mesh truncation setup.

the rate of convergence achieved. The result shown has been obtained with a plane wave excitation from $(\theta^{\text{inc}}, \phi^{\text{inc}}) = (0°, 0°)$. Very similar results are obtained with other angles of incidence. In order to show the latter, the convergence behavior for different angles of incidence and a given case of mesh truncation setup (specifically, the case labeled as $\mathcal{T}_2$) is shown in Figure 5. It is observed how the rate of convergence is virtually independent of the angle of incidence when a convex truncation boundary S is used.

The rest of results shown in the paper correspond to the non-convex truncation boundary case. A number of different non-convex

cases with different overlapping between Ω^{FEM} and Ω^{EXT}, i.e., distance between S and S' surfaces, have been analyzed. In the following, two relevant cases (named as $\mathcal{A}$ and $\mathcal{B}$ in the following) are considered. They correspond to $\triangle_S$ equal to 0.1λ and 0.15λ, respectively (see Table 2(b)).

The convergence curves of these two cases are shown in Figures 6 and 7, respectively, where the change of the residual error (normalized), between two consecutive iterations along the 50 first iterations, is depicted. The structure is illuminated by a plane wave at incidence angle (θ^{inc}, ϕ^{inc}). The first 5 eigenvalues for the two cases under study are shown in Table 3. The eigenvalues are computed using the library ARPACK [20], which is based on the so named *Implicitly Restarted Arnoldi Method* (IRAM). The first observation is that the method converges for the case $\mathcal{A}$ and diverges for $\mathcal{B}$. This observation agrees

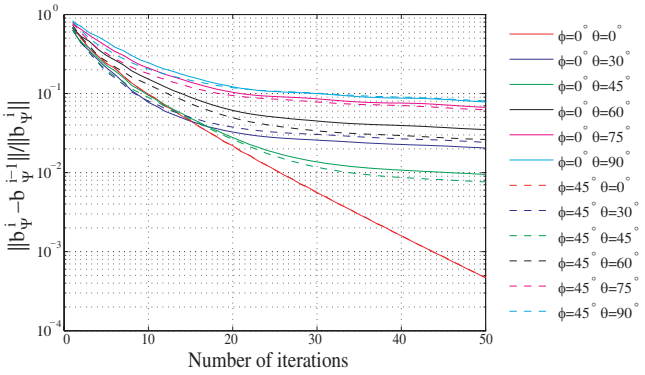

Figure 6. Convergence for the case $\mathcal{A}$. $\Delta_S = 0.1\lambda$.

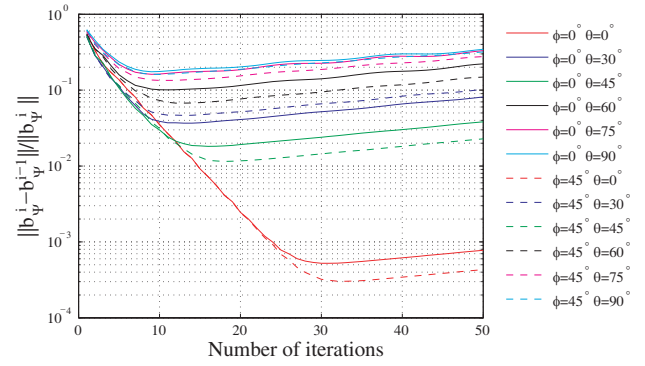

Figure 7. Convergence for the case $\mathcal{B}$. $\Delta_S = 0.15\lambda$.

Table 3. Eigenvalues with greatest absolute value.

	$\mathcal{A}$	$\mathcal{B}$
1	0.9896	1.0234
2	0.8849	0.9215
3	0.8846	0.7767
4	0.8311	0.7750
5	0.8305	0.7656

with the spectral radius of the cases under consideration (see Table 3). It is worth noting that an increment of the overlapping region for non-convex truncation boundaries does not imply a faster convergence as it is observed when a convex truncation boundary is used. Actually, an increase of the overlapping region leads to the divergence of the method in this example.

It can be also noticed that the rate of convergence depends on the incidence angle of the plane wave that illuminates the cavity. The rate of convergence is faster when the illumination is from $\theta^{\text{inc}} = 0^\circ$ for the two cases. The rate slows down for grazing angles (close to 90°). This is due to the fact that the multiple reflections between the internal walls of the cavity are not well modelled by the Cauchy local approximation imposed on the boundary S. These reflections produce the excitation of a resonant field pattern inside the cavity, as it will be shown later.

Another observation, obvious from the definition of the iteration matrix from (11), is that the spectral radius of the iteration matrix does not depend on the incidence angle. Moreover, it can be noticed one or two lineal zones in each convergence curve with an associated slope. The slope of the curve has a direct relation with the projection of the change of the residual error, between two consecutive iterations, onto a given eigenvector. The correspondence between the slopes in the lineal zones of the convergence curves and one of the eigenvalues of the iteration matrix is as follows:

$$\lambda = e^{\frac{\ln\left(\left|z^{(i)}\right|/\left|z^{(j)}\right|\right)}{i-j}} \tag{21}$$

where $i > j$. Thus, in the case $\mathcal{A}$ and incidence angle $\theta^{\text{inc}} = 0^\circ$, between the iterations $j = 20$ and $i = 50$, a value of $\lambda = 0.87964$ is obtained using (21), that is close to the second and third eigenvalue (see Table 3). For other incident angles, the last zone is lineal and the slopes are practically parallel between them. For instance, for $(\theta^{\text{inc}}, \phi^{\text{inc}}) = (75^\circ, 0^\circ)$, and between $j = 25$ and $i = 50$ iterations, a

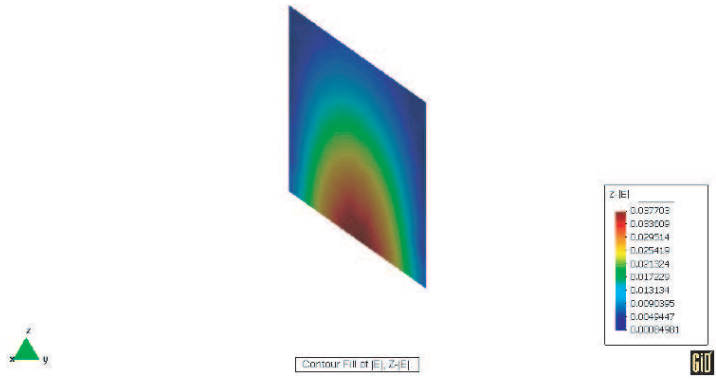

Figure 8. Magnitude $|E_z|$ in the interior of the cavity when the problem is excited by the first eigenvector in the case $\mathcal{A}$. Plane yz.

value of $\lambda = 0.98752$ is obtained (very close to the first eigenvalue). If the problem is excited with the eigenvector associated to this eigenvalue (the one that limits the convergence of the method), i.e.,

$$\left\{\phi^{(0)}\right\} = [K]^{-1} \begin{Bmatrix} 0 \\ \{v_1\} \end{Bmatrix} \tag{22}$$

a resonant field pattern is observed for the "error field" inside the cavity, as it is depicted in Figure 8. Note that expression (22) is obtained from (12) by substitution of $\{b^{(0)}_{\Psi_e}\}$ by $\{v\}_1$ and making $\{\phi_t\} = 0$. For the rest of cases and incidence angles, similar considerations can be made.

In order to better illustrate how the excitation of the dominant resonant-type mode depicted in Figure 8 occurs depending on the incidence angle, consider the results shown in Figures 9–12. In these figures, the projection of the change of the residual error, between two consecutive iterations, $(\mathbf{z}^{(i)})$, on the eigenvectors space (spanned by $\mathbf{v}_j$) are shown for the mesh truncation cases $\mathcal{A}$ and $\mathcal{B}$, and incidence angles ($\theta = 0°$, $\phi = 0°$) and ($\theta = 75°$, $\phi = 0°$).

With respect to Figure 9, it can be noticed that for the first iteration the main contribution to the residual error comes from the 14th eigenvector ($|c_{14}| > |c_j| \; \forall j \neq 14$). However, its associated eigenvalue $\lambda_{14} = 0.5967$ (not shown in Table 3) is small enough such that its contribution to the error after a few iterations ($|c_{14}| \cdot |\lambda_{14}|^{(i-1)}$ for the i-th iteration) is negligible. After a few iterations the second and third eigenvalues ($\lambda_3 \approx \lambda_4$, see Table 3) govern the rate of convergence. It is worth noting that although not observed in Figure 6, the rate of convergence is expected to change after approximately 60 iterations

(residual error around 10^{-4}) due to the contribution of first eigenvalue. In practice, the value of λ_1 is so close to one that the convergence has virtually stagnated after that point. Comparing the results of Figure 9 with the ones depicted in Figure 10, it can be observed that the main difference between the two is the higher excitation of the first eigenvector in the latter case that produces the stagnation phenomenon at an error level around 10^{-1}. The first eigenvector field corresponds, as shown in Figure 8, to a resonance field between the in front walls of the cavity. This type of mode is significantly excited for grazing

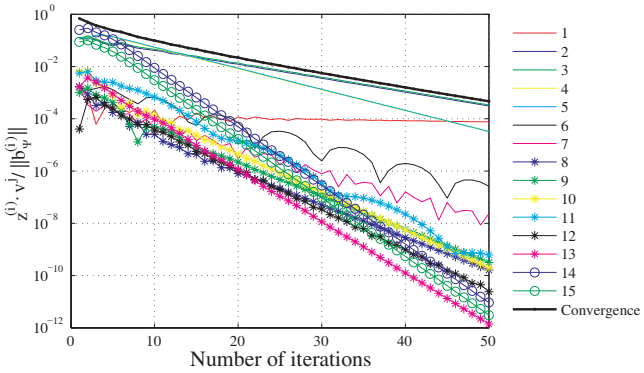

Figure 9. Projection of the 15 first eigenvectors over the change of the residual error for the case $\mathcal{A}$ and incidence angle ($\theta = 0°$, $\phi = 0°$) in each iteration.

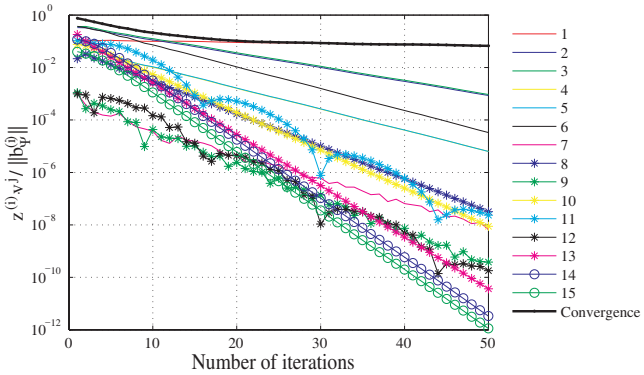

Figure 10. Projection of the 15 first eigenvectors over the change of the residual error for the case $\mathcal{A}$ and incidence angle ($\theta = 75°$, $\phi = 0°$) in each iteration.

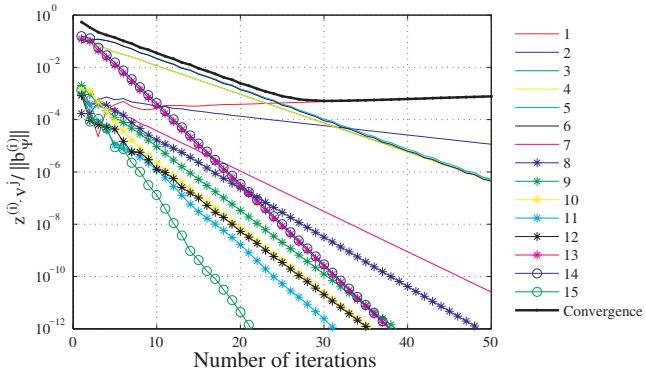

Figure 11. Projection of the 15 first eigenvectors over the change of the residual error for the case $\mathcal{B}$ and incidence angle ($\theta = 0°$, $\phi = 0°$) in each iteration.

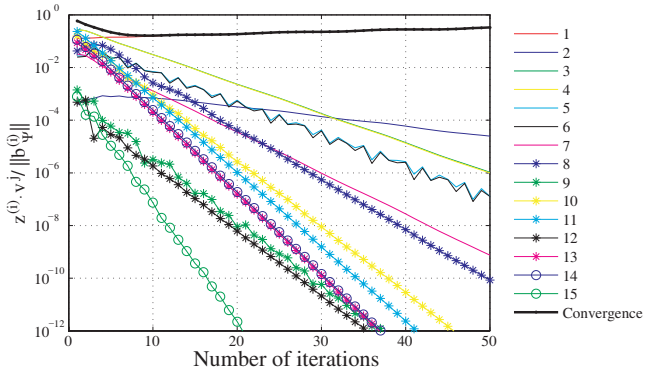

Figure 12. Projection of the 15 first eigenvectors over the change of the residual error for the case $\mathcal{B}$ and incidence angle ($\theta = 75°$, $\phi = 0°$) in each iteration.

angles. Therefore, it is expected to be excited with higher levels for $\theta^{\text{inc}} = 75°$ than $\theta^{\text{inc}} = 0°$.

The same type of results as those above, but for the case of mesh truncation $\mathcal{B}$, are shown in Figures 11 and 12. As in case $\mathcal{A}$, the excitation of the first eigenvector c_1 is larger for $\theta^{\text{inc}} = 75°$ than $\theta^{\text{inc}} = 0°$; actually, with similar values to the ones of case $\mathcal{A}$. The main difference is that its associated eigenvalue λ_1 is greater than one in this case. That makes the method diverge instead of stagnate.

It is worth noticing again here that the spectral radius is independent on the angle of excitation. The differences between

exciting from one angle of incidence or another comes from the different amounts of excitation of the eigenvectors of slow convergence. Although truncation cases $\mathcal{A}$ and $\mathcal{B}$ might be used in practice to analyze the problem with excitation angles close to $\theta^{\text{inc}} = 0^{\circ}$ (errors around 10^{-4} are beyond the limits of engineering accuracy for most applications), it is difficult to predict for an arbitrary structure the error level (or iteration number) in which the stagnation/divergence can occur. Thus, the only robust procedure in general is to use convex-mesh truncation boundaries, i.e., to mesh the region between the cavity walls.

It is worth noting that no guarantee of better convergence exists when making the S-S' distance larger for the case of a non-convex truncation boundary; an example is the comparison between cases $\mathcal{A}$ and $\mathcal{B}$ shown in this paper. Other truncation cases (not shown in the paper) have been studied and a clear pattern of when convergence/divergence happens has not been detected.

4. CONCLUSIONS

A convergence study of a non-standard Schwarz domain decomposition method with overlapping for finite element mesh truncation in electromagnetics has been presented. The main objective has been to gain insight into the convergence behavior of the method for non-convex truncation boundaries. The problem of the scattering of a cavity type metallic object by a plane wave has been considered. The spectrum of the iteration matrix for different truncation boundaries has been computed. It is concluded that a clear pattern about how the method diverges or converges depending on the size of the overlapping region cannot be obtained for the case of a non-convex truncation boundary. Although in some situations the convergence is assured because the spectral radius may be (strictly speaking) smaller than one, the method in practice stagnates after reaching a certain error level. The field solutions corresponding to the dominant eigenvectors (those associated to eigenvalues close or greater than one) have been obtained. A resonant field pattern on the reentrant part of the structure (due to the strong coupling between the cavity walls) is observed. The Cauchy type boundary condition simply cannot accurately take into account of those interactions. The dependence of the excitation of the dominant eigenvector fields with the incidence angle has been studied. As expected, the illumination with grazing angles provide a significant excitation of those eigenvector fields and the stagnation/divergence behavior is reached before (higher error levels) than with angles close to broadside. The projection of the change of the residual error on the

eigenvectors space has been computed. The numerical results clearly match and explain the convergence plots obtained.

ACKNOWLEDGMENT

This work has been supported by the Ministerio de Educacion y Ciencia, Spain, under Projects TEC2007-65214/TCM and TEC2010-18175/TCM.

REFERENCES

1. Jin, J. M., *The Finite Element Method in Electromagnetics*, 2nd edition, John Wiley & Sons, Inc., 2002.
2. Salazar-Palma, M., T. K. Sarkar, L. E. García-Castillo, T. Roy, and A. R. Djordjevic, *Iterative and Self-Adaptive Finite-Elements in Electromagnetic Modeling*, Artech House Publishers, Inc., Norwood, MA, 1998.
3. Ping, X. W. and T.-J. Cui, "The factorized sparse approximate inverse preconditioned conjugate gradient algorithm for finite element analysis of scattering problems," *Progress In Electromagnetics Research*, Vol. 98, 15–31, 2009.
4. Tian, J., Z.-Q. Lv, X.-W. Shi, L. Xu, and F. Wei, "An efficient approach for multifrontal algorithm to solve non-positive-definite finite element equations in electromagnetic problems," *Progress In Electromagnetics Research*, Vol. 95, 121–133, 2009.
5. Harrington, R. F., *Field Computation by Moment Methods*, IEEE Press, 1993.
6. Wang, S., X. Guan, D.-W. Wang, X. Ma, and Y. Su, "Electromagnetic scattering by mixed conducting/dielectric objects using higher-order MoM," *Progress In Electromagnetics Research*, Vol. 66, 51–63, 2006.
7. Liu, Z.-L. and J. Yang, "Analysis of electromagnetic scattering with higher-order moment method and NURBS model," *Progress In Electromagnetics Research*, Vol. 96, 83–100, 2009.
8. Taboada, J. M., M. G. Araujo, J. M. Bertolo, L. Landesa, F. Obelleiro, and J. L. Rodriguez, "MLFMA-FFT parallel algorithm for the solution of large-scale problems in electromagnetics," *Progress In Electromagnetics Research*, Vol. 105, 15–30, 2010.
9. García-Castillo, L. E., I. Gómez-Revuelto, F. Sáez de Adana, and M. Salazar-Palma, "A finite element method for the analysis of radiation and scattering of electromagnetic waves on complex

environments," *Computer Methods in Applied Mechanics and Engineering*, Vol. 194, Nos. 2–5, 637–655, Feb. 2005.

10. Fernández-Recio, R., L. E. García-Castillo, I. Gómez-Revuelto, and M. Salazar-Palma, "Fully coupled hybrid FEM-UTD method using NURBS for the analysis of radiation problems," *IEEE Transactions on Antennas and Propagation*, Vol. 56, 774–783, Mar. 2008.
11. Fernández-Recio, R., L. E. Garcíá-Castillo, I. Gómez-Revuelto, and M. Salazar-Palma, "Fully coupled multi-hybrid FEM-PO/PTD-UTD method for the analysis of scattering and radiation problems," *IEEE Transactions on Magnetics*, Vol. 43, 1341–1344, Apr. 2007.
12. Vouvakis, M. N., K. Zhao, S. M. Seo, and J.-F. Lee, "A domain decomposition approach for non-conformal couplings between finite and boundary elements for unbounded electromagnetic problems in R^3," *Journal of Computational Physics*, Vol. 225, No. 1, 975–994, 2007, doi:10.1016/j.jcp.2007.01.014.
13. Paul, P. and J. P. Webb, "Balancing boundary and discretization errors using an iterative absorbing boundary condition," *IEEE Transactions on Magnetics*, Vol. 44, 1362–1365, Jun. 2008.
14. Paul, P. and J. P. Webb, "Reducing computational costs using a multi-region finite element method for electromagnetic scattering," *IET Microwaves, Antennas & Propagation*, Vol. 2, No. 5, 427–433, 2008, doi:10.1049/iet-map:20070227.
15. Zhao, K., V. Rawat, and J.-F. Lee, "A domain decomposition method for electromagnetic radiation and scattering analysis of multi-target problems," *IEEE Transactions on Antennas and Propagation*, Vol. 56, 2211–2221, Aug. 2008.
16. Wang, X., Z. Peng, and J.-F. Lee, "Simulation of the mutual couplings among multiple antennas on large platform using multi-region multi-solver domain decomposition," *IEEE Antennas and Propagation Society International Symposium Digest*, 1–4, Institute of Electrical and Electronics Engineer (IEEE), Toronto, Canada, USA, Jul. 2010.
17. Alfonzetti, S., G. Borzi, and N. Salerno, "Iteratively-improved Robin boundary conditions for the finite element solution of scattering problems in unbounded domains," *International Journal for Numerical Methods in Engineering*, Vol. 42, 601–629, 1998.
18. Fernández-Recio, R., L. E. Garcia-Castillo, I. Gómez-Revuelto, and M. Salazar-Palma, "Convergence study of a non-standard schwarz domain decomposition method for finite element mesh

truncation in electromagnetics," *International Conference on Electromagnetics in Advanced Applications (ICEAA07)*, Torino (Italia), Sept. 2007. Invited paper to the Special Session "Numerical Methods in Electromagnetics".

19. García-Castillo, L. E. and M. Salazar-Palma, "Second-order Nédélec tetrahedral element for computational electromagnetics," *International Journal of Numerical Modelling: Electronic Networks, Devices and Fields*, Vol. 13, 261–287, John Wiley & Sons, Inc., Mar.–Jun. 2000.
20. Lehoucq, R. B., D. C. Sorensen, and C. Yang, *ARPACK Users'Guide: Solution of Large Scale Eigenvalue Problems with Implicitly Restarted Arnoldi Methods*, 1997, http://people.scs.fsu.edu/~burkardt/pdf/arpack.pdf.